Research Article

Journal of Environmental Nanotechnology

Enhanced NO_2 Gas Sensing Using Ce-doped ZnO Nanostructures

Bahaa Fakhry Shehab[1], Aneed Maher Lafta[2] and Zaid L. Hadi[3*]

[1]Ministry of Education, General Directorate of Education of Rusafa II, BGW, Iraq
[2]Ministry of Education, General Directorate of Education of Tikrit, Tikrit, Iraq
[3]Ministry of Education, General Directorate of Education of Babylon, Babel, Iraq
Received: 26.07.2025 Accepted: 03.09.2025 Published: 30.09.2025
*zaid.altai@outlook.com

ABSTRACT

This study investigates the NO_2 gas detection capabilities of cerium-doped zinc oxide and the effects of varying the cerium concentration. The experiment utilized spray pyrolysis, X-ray diffraction (XRD), and infrared (IR) spectroscopy, along with a mesh aluminum electrode, on thin film samples. Thermocouples monitored the heat variance with gas levels inside a sealed gas chamber using an internal gas sensor, and the sample resistance was continuously measured and recorded. XRD analysis of ZnO nanostructures revealed a hexagonal wurtzite crystal structure with distinct alignment along specific crystallographic planes. The introduction of Ce dopants caused a red shift in the absorption edge of ZnO toward higher wavelengths, extending its absorption into the visible light spectrum. The bandgap value was shifted via doping, which showed for ZnO and Ce/ZnO were 3.32, 3.24, and 3.22 eV, respectively. The FTIR spectrum revealed the presence of hydroxyl groups (OH) associated with water molecules, which can be attributed to the combined influence of two overlapping vibrational modes. The NO_2 gas is a byproduct of chemical operations, with a vibrational wavenumber of 1526 cm^{-1}. The discernible fingerprint bond of Ce–O was identified as a stretching vibration in the range of 740 cm^{-1} and 655 cm^{-1}. The position of the Zn–O stretching vibration band varies depending on factors such as the dimensions, structure, and crystallinity of the ZnO nanoparticles. The gas sensing data were obtained using methods capable of detecting concentrations as low as 10 to 100 ppm. The specimen containing 10% Ce/ZnO exhibited the highest sensitivity among all samples.

Keywords: ZnO; Ce/ZnO; Thin films; Gas sensing; Spray pyrolysis.

1. INTRODUCTION

Doping can improve the physical properties of thin zinc oxide (ZnO) films (Shukla *et al.* 2013). Since cerium-doped ZnO has distinct characteristics, it is widely used as a gas sensor (Lu *et al.* 2017). Air pollution has increased dramatically because of industrialization and urbanization. Nitrogen dioxide is a noxious gas with a strong, pungent odor and is considered poisonous. In humans, exposure to ppm levels of NO_2 has been shown to cause harm to one's health (Manisalidis *et al.* 2020). Developing highly sensitive and selectively improved sensors for NO_2 gas is crucial, but it presents significant challenges (Sun *et al.* 2023). NO_2 is a red-brown oxidizing gas noted for its irritating properties (Orellano *et al.* 2020). It is primarily a hazardous pollutant resulting from transportation and combustion reactions that occur in industrial activities. The gas-sensing response of the NiO-MnO2 nanosheet sensor reached a notable value of 165 when detecting 100 ppm hydrogen sulfide gas (Saranya *et al*. 2024). Recently, academic researchers have shown interest in ZnO gas sensors due to their exceptional thermal stability and high carrier mobility (Diao *et al.* 2018). In addition, doping ZnO sensors has been identified as a viable strategy for improving their gas-detection capability by manipulating their local structure and coordination environment (Kulandaisamy *et al.* 2016). ZnO is classified as an n-type semiconductor characterized by its wide band gap and notable electron mobility. ZnO thin films have been demonstrated in various applications, including gas sensing. ZnO sensors can detect various gases, including nitrogen dioxide, carbon monoxide, and ammonia (Chai *et al.* 2014). The field of gas sensors has seen significant focus on materials based on cerium oxide (CeO_2) (Li *et al.* 2021). Recently, there has been growing interest in using CeO_2 as a gas sensor. This material detects various gases, including ammonia, acetone, ethanol, formaldehyde, and carbon monoxide (Hussain *et al.* 2018). Doping CeO_2 and ZnO materials has been the subject of numerous inquiries, primarily due to the encouraging results observed in gas sensing applications. Compared to CeO_2, ZnO exhibits a larger bandgap. As a result, the combination of these two oxides produces metal oxide structures with adjustable physical properties (Srinivasan *et al.* 2023). Previous research has shown that transition metal oxides have many phases or component minerals. These include CuO-NiO (Sui *et al.* 2020), ZnO-CuO (Zhang *et al.* 2016), NiO – ZnO (Kim *et al.* 2017), ZnO-ZnSe (Gao *et al.* 2023), and CdTe-ZnO (Jaiswal *et al.* 2021). It was reported that these couplings were employed in various applications, including catalysis,

sensors, and dielectrics. Despite this, rare-earth metals in oxide form have distinctive structural, optical, and morphological characteristics. There is much interest in the interaction between rare earth metals and transition metal oxides (Srinivasan *et al.* 2023). Ce-doped ZnO synthesis has previously been documented using various methods, including Spray Pyrolysis (Sofiani *et al.* 2006), Sol-gel (Akbari *et al.* 2017), Magnetron Sputtering (Heng *et al.* 2016), Hybridized Hydrothermal (Reddy *et al.* 2016), Solid Stabilized Emulsion (He *et al.* 2006), Electrodeposition, Soft Solution (Li *et al.* 2002), Microwave-assisted Synthesis (Shulga *et al.* 2020), and others. Rare earth elements possess distinctive electronic structures and exhibit various energy levels. Therefore, using rare earth elements as dopants in ZnO materials has shown promising potential for photoelectric devices. Consequently, experimental and theoretical investigations have received significant attention in this area of research (Mary *et al.* 2014; Mary *et al.* 2015; Verma and Kotnala, 2016; Zhang *et al.* 2011). This study examines the gas detection capabilities of Ce/ZnO in the detection of NO_2, as well as the effects of varying the cerium concentration.

2. MATERIALS AND METHODS

The deposition of ZnO onto the glass substrate was carried out using a spray pyrolysis setup. The glass substrates were cleaned using ultrasonic acetone for 25 minutes and then washed with deionized water. Then, the substrates were positioned on a plate heated to a temperature of 350 °C, with an accuracy level of 5 °C. A thin material layer is applied to the substrate, which is heated within a controlled deposition chamber. The system's temperature gradually reduced to the ambient temperature after completely exhausting the substrate's resources. The precursor salt employed in this investigation was zinc acetate dihydrate ($Zn(CH_3COO)_2.2H_2O$), obtained from Sigma-Aldrich with a purity of 99.99%. During this experiment, the precursor salt was solubilized in a solution containing 100 ml of deionized water. The spraying gun was raised 30 cm above the substrate. Dispersing a precursor solution into a fine mist was accomplished using compressed air as a carrier gas. The experimental parameters were: a flow rate of 2 ml/min, a spray interval of 5 s, a break time of 10 s, and 200 cycles. Several atomic ratios were used during spraying to achieve the desired results. X-ray diffraction patterns were recorded *via* the Japanese Shimadzu XRD 6000 X-ray Diffractometer for microstructural analysis. A Bragg angle between 30° and 60° was used to record the diffraction pattern in conjunction with XRD. The Shimadzu SP-8001 computerized spectrometer gathered the optical data from UV to near infra-red regions. JEOL Ltd.'s JSM-7600F Scanning Electron Microscope was used to examine surface morphology. Energy-dispersive X-ray spectroscopy was employed to investigate stoichiometry. An IR Prestige-21 Shimadzu was used in this study for IR spectroscopy. A mesh aluminum electrode is deposited on thin film samples using the Edward Coating System by thermal evaporation. By utilizing an internal sensor, thermocouples are able to measure temperature depending on the levels of gas that are present within a gas chamber that is hermetically sealed and is positioned on a heated plate. The oxidizer gas was used as an oxidizing agent in the gas-filled room designated for this purpose. The sample resistance was continuously measured and recorded with a multimeter connected to a laptop.

3. RESULTS AND DISCUSSION

The analysis included recording and plotting XRD data on the same intensity scale for clarity, as well as evaluating the FWHM, d-spacing, crystallite size, and crystal planes (*hkl*). The XRD investigations reveal that the diffraction peaks observed in the ZnO nanostructures were consistent with the conventional diffraction peaks associated with hexagonal ZnO. Consequently, it can be observed that nanostructures universally exhibit a hexagonal wurtzite crystal structure, displaying a distinct inclination towards alignment along specific crystallographic planes, namely (100), (002), (101), (102), and (110). According to the literature, the mineral name for ZnO patterns is Zincite (Xu and Ching, 1993), and the corresponding crystallographic card number is (96-901-1663). Reflection angles of 32.09°, 34.52°, 36.39°, 47.67°, and 56.90° are indicated here. The XRD results were in good agreement with the literature (Naqvi *et al.* 2014). The introduction of Ce doping into the ZnO crystal structure did not disrupt or alter the crystal lattice. Furthermore, no secondary or impurity phases were seen as a result of the Ce doping process. However, Ce doping affected diffraction peak intensity and position, as shown by prior study (Akçay *et al.* 2023). Simultaneously, the element Ce was observed to manifest as CeO_2 in a cubic crystalline phase, as indicated by crystallographic card No. 96-434-3162 (Artini *et al.* 2015). The CeO_2 material exhibited peak intensities at the (111) and (200) crystallographic planes. The magnitude of the diffraction peaks is contingent upon the level of Ce doping. The diffraction angles corresponding to the (100), (002), (101), (102), and (110) crystallographic planes showed variations in samples with 10% and 20% Ce doping, as presented in Table 1.

Fig. 1 depicts the XRD patterns of the deposited Ce/ZnO thin films. The analysis revealed the presence of Ce at a concentration of 0.1, with a diffraction angle (2θ) of 28.06° corresponding to (111) crystallographic planes. At a Ce concentration of 0.2, the diffraction angles (2θ) for the (111) and (200) planes were measured to be 27.93° and 32.74°, respectively. The X-ray diffraction (XRD) findings were consistent with the information provided in the sources (Sharma *et al.* 2016).

Table 1. XRD parameters of ZnO films deposited at different Ce/ZnO concentrations

	2θ (deg.)	FWHM (deg.)	D_{hkl} (Å)	C.S. (nm)	*hkl*	Phase
ZnO	32.09	0.7037	2.8067	11.8	(100)	Hex. ZnO
	34.52	0.9786	2.5959	8.5	(002)	
	36.39	0.7052	2.4715	11.9	(101)	
	47.67	1.4477	1.9095	7.6	(102)	
	56.90	0.8996	1.6154	11.2	(110)	
(0.1) Ce/ZnO	31.96	0.7433	2.8067	11.1	(100)	Hex. ZnO
	34.51	0.8216	2.5966	10.1	(002)	
	36.42	0.7436	2.4715	11.3	(101)	
	47.62	1.5257	1.9095	7.6	(102)	
	56.93	0.8997	1.6154	11.2	(110)	
	28.06	1.4083	3.1773	5.8	(111)	Cub. CeO_2
(0.2) Ce/ZnO	31.99	0.6654	2.7948	12.4	(100)	Hex. ZnO
	34.38	0.7825	2.6059	10.6	(002)	
	36.45	0.7044	2.4626	11.9	(101)	
	47.53	1.1346	1.9095	7.6	(102)	
	56.88	0.9781	1.6154	11.2	(110)	
	27.93	0.7041	3.1915	11.6	(111)	Cub. CeO_2
	32.74	0.5479	2.7325	15.1	(200)	

As evident from Table 1, there is much agreement between the observed and reported d-spacing values. According to calculations that agree with the references, the collected d-spacing values were observed with approximately 96% accuracy (Xin *et al.* 2022; Moslehnejad *et al.* 2022). The FWHM analysis of the XRD spectrum was also conducted to determine the crystallite size (D). Scherrer's formula (Debye and Scherrer, 1916) was applied to predict the average crystallite size, as shown in Eq. 1.

$$D_{hkl} = \frac{K\lambda}{\beta \cos(\theta_{hkl})} \quad \ldots (1)$$

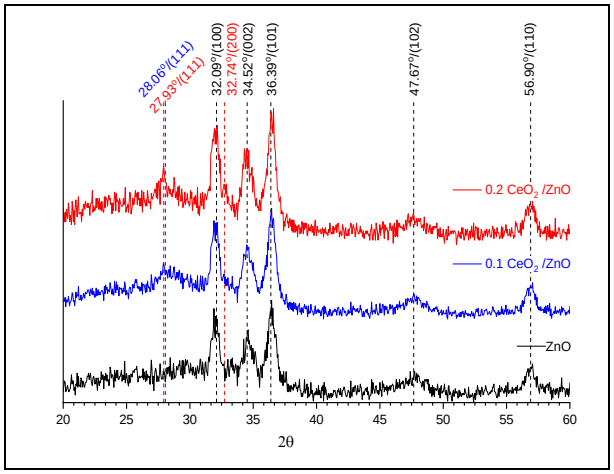


Fig. 1: XRD patterns for ZnO and (0.1, 0.2) CeO_2-deposited films

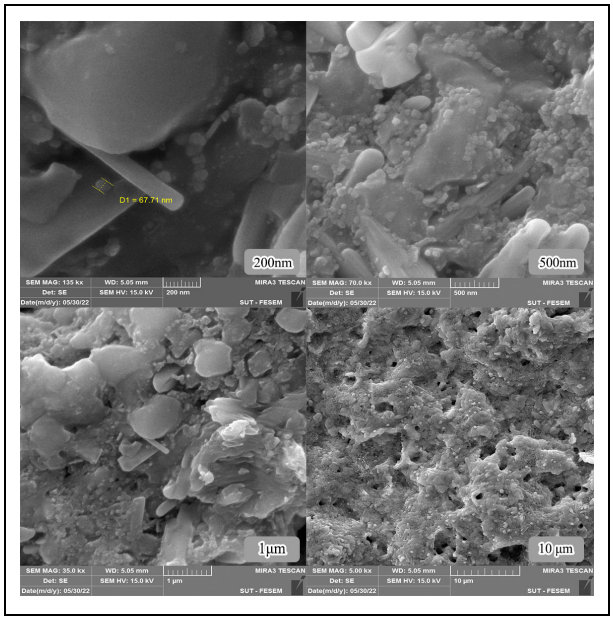


Fig. 2: FE-SEM images of ZnO-deposited thin films

The surface properties of pure ZnO nanostructures are depicted graphically in Fig. 2.

The clusters of extremely small rod-shaped structures are visible in the SEM micrograph of undoped ZnO. These ZnO particles have a diameter of roughly 68 nm. The shape of the Ce/ZnO is illustrated in Fig. 3. It is important to point out that a unique nanostructure was discovered at the Ce (0.1) level.

The measured thicknesses of the deposited films ranged from 194 to 202 nm, as determined by the Fizeau method (Buckman and Kuo, 1978), which involved the deployment of a green laser with a wavelength of 532 nm.

Numerous studies have examined the UV-Vis absorption spectra of Ce/ZnO. As evident from Fig. 4, these spectra provide information about the light absorption by the Ce/ZnO composite material in the UV and visible regions of the electromagnetic spectrum. The absorption properties of Ce/ZnO have been demonstrated to undergo alterations in the UV-Vis absorption spectra when compared to those of pure ZnO. The introduction of Ce dopants can shift the absorption edge of ZnO towards higher wavelengths, thereby extending its absorption into the visible light spectrum. This phenomenon, known as a 'red shift', refers to the displacement of the absorption spectrum towards longer wavelengths within the visible range.

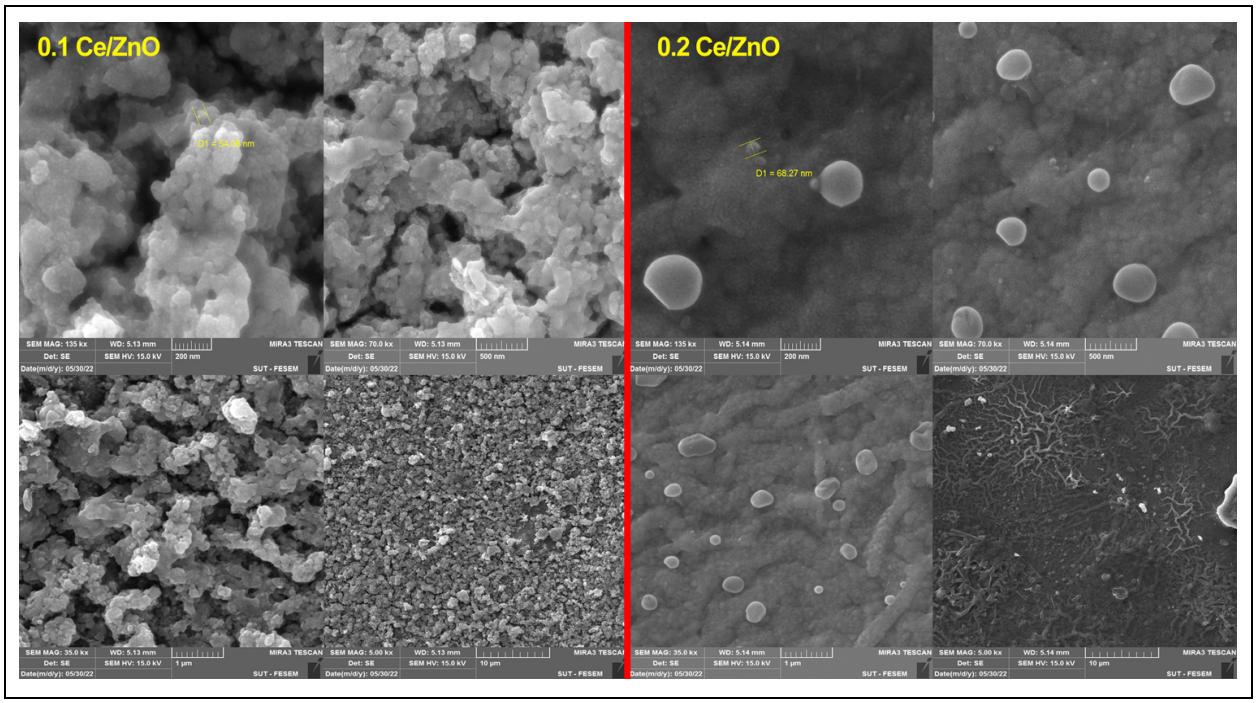


Fig. 3: FE-SEM images of 0.1 and 0.2 Ce/ZnO thin films

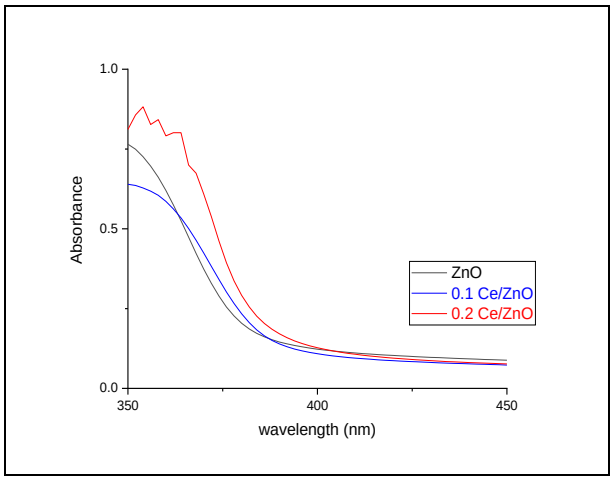


Fig. 4: Absorption spectrum of ZnO and Ce/ZnO samples

The Tauc formula (Tauc *et al.* 1966) was utilized to display $(\alpha h\nu)^2$ relative to $(h\nu)$. Based on bandgap calculations, the results of this plot may be found in Fig. 5. The bandgap values of ZnO and 0.1 and 0.2 Ce/ZnO were found to be 3.32, 3.24, and 3.22 eV, respectively, as shown in Fig. 5. The findings align with those reported by Prakoso *et al.* 2016.

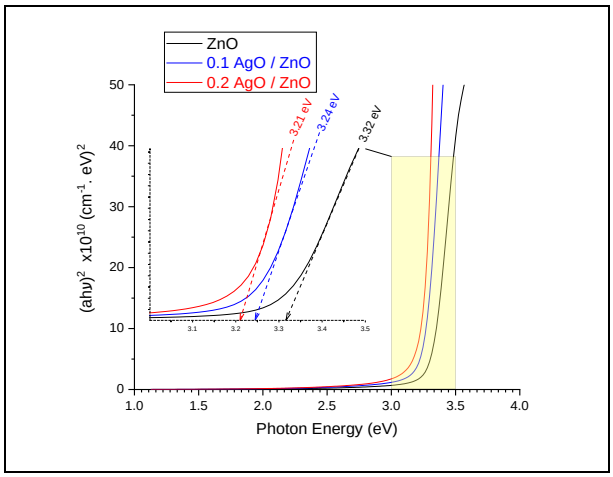


Fig. 5: Description of energy bandgap of ZnO and Ag/ZnO thin films

Fig. 6 depicts the FTIR spectra of Ce/ZnO samples. The band located at 3577–3383 cm^{-1} indicates the presence of hydroxyl groups (OH) associated with water molecules (Elderderi *et al.* 2020), and corresponds to scissoring bending vibrations, exhibiting distinct sharpness and moderate intensity. The observed phenomenon can be attributed to the combined influence of two vibrational modes that overlap, namely the symmetrical and asymmetrical stretching modes of the H_2O molecules. The inherent intensity of stretching modes in infrared spectra also plays a role in this outcome. The C-H stretching frequencies at 3063 cm^{-1} and 2994 cm^{-1} (Mihály *et al.* 2017) correspond to the stretching mode of the C-H bond, whereas the frequency of 2857 cm^{-1} (Ghalmi *et al.* 2019) indicates the vibration of the CH_2 group. Hydrogen-bonded groups may be attributed to the absorptions at 1686 cm^{-1} (Bao *et al.* 2006).

NO_2 gas is a byproduct of chemical operations and has a vibrational frequency of 1526 cm^{-1} (Petruci *et al.* 2019), C-H bending at 1329 cm^{-1}, and C-O stretching at 1177 cm^{-1} (Nandiyanto *et al.* 2019). The discernible fingerprint bond of Ce-O was recognized as a stretching frequency in the range of 740–655 cm^{-1} (Grinter *et al.* 2021; Fifere *et al.* 2022). In addition to the regular Ce-O bond, a Ce=O double bond can be formed in cerium complexes. The location of the ZnO stretching vibration band can exhibit variability based on factors such as the dimensions, structure, and degree of crystallinity of the ZnO nanoparticles. Typically, a decrease in particle size and an increase in crystallinity result in a shift towards lower wavenumbers (corresponding to higher frequency) for the peak location. This phenomenon is attributed to the shorter ZnO bond length observed in smaller particles and the increased rigidity exhibited by more crystalline particles. Babu *et al.* (2013) and Chen *et al.* (2018) reported the manifestation of the Zn-O bond in the metal oxide material by detecting characteristic peaks in the FTIR fingerprint area at 454 cm^{-1} and 404 cm^{-1}.

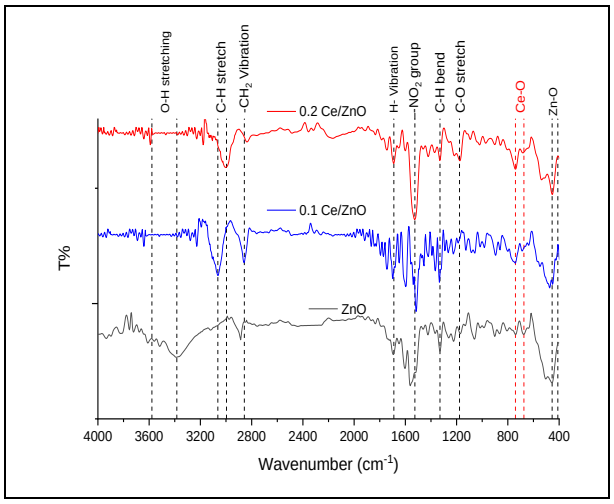


Fig. 6: FTIR spectroscopy of Ce/ZnO samples

The Ce/ZnO nanostructure surface controls the detection of gases as part of the sensing process. Meanwhile, chemisorbed oxygen adds some friction to the surface. However, the reaction mechanism of NO_2 is quite intricate, involving several stages. As shown in Fig. 7, Ce/ZnO samples react with NO_2. The experimental measurements were conducted at three discrete operating temperatures (100°C, 200°C, and 300°C), with their respective response and recovery times recorded. The gas sensing data were obtained using methods that allowed for low detection limits ranging from 10 to 100 ppm.

Table 2 presents the gas sensing analysis findings, including the response time and recovery time observed at the designated operating temperature. Furthermore, the sensitivity (*S%*) of the samples produced was determined by employing Eq. 2 (Tsai *et al.* 2018).

$$S\% = \frac{R_{gas} - R_{air}}{R_{air}} \, x \, 100 \qquad \ldots (2)$$

As per the equation, the variables R_{air} and R_{gas} represent the resistance of the deposited sample in ambient air and when exposed to a specific gas under examination, respectively.

Table 2. Gas sensing characteristics (sensitivity, response time, and recovery time)

Sample	Temperature (°C)	Sensitivity %	Response Time (s)	Recovery Time (s)
ZnO	200	16.7	20.0	60.0
	250	31.0	25.0	40.0
	300	24.9	20.0	30.0
0.1 Ce / ZnO	200	5.10	20.0	50.0
	250	15.8	20.0	60.0
	300	35.4	20.0	40.0
0.2 Ce / ZnO	200	22.7	15.0	60.0
	250	33.3	22.0	80.0
	300	17.0	30.0	70.0

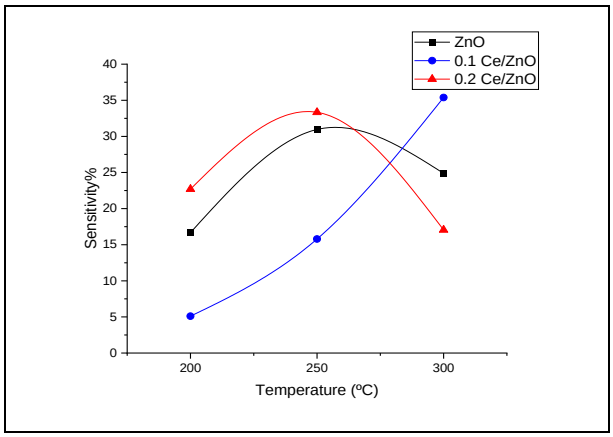


Fig. 7: Sensitivity of samples at different temperatures

Fig.. 7 depicts the variations in conductivity seen throughout the gas test. It can be observed that the specimen with a composition of 10% Ce/ZnO exhibits the highest level of sensitivity compared to all the other samples.

4. CONCLUSION

This study investigated the use of cerium-doped zinc oxide films as gas sensors for detecting nitrogen dioxide. The study employed Spray pyrolysis, XRD, IR spectroscopy, and a mesh aluminum electrode on thin-film samples to analyze the gas detection capabilities of Ce/ZnO thin films. The results showed a hexagonal wurtzite crystal structure with crystallographic plane alignment, and Ce dopants were found to shift the ZnO absorption edge towards higher wavelengths, enhancing visible light absorption. The FTIR spectrum indicated the presence of hydroxyl groups on water molecules due to two overlapping vibrational modes. The stretching frequencies of the Ce–O fingerprint bond were 740 cm^{-1} and 655 cm^{-1}. The size, structure, and crystallinity of ZnO nanoparticles influence the position of the Zn–O stretching vibration band. Methods with modest detection limits (10–100 ppm) were used to collect gas sensing data, and the 10% Ce/ZnO sample was identified as the most sensitive. The study highlighted the potential of Ce/ZnO in photoelectric devices and the role of Ce dopants in enhancing gas sensing capabilities.

FUNDING

This research received no specific grant from any funding agency in the public, commercial, or not-for-profit sectors.

CONFLICTS OF INTEREST

The authors declare that there is no conflict of interest.

COPYRIGHT

This article is an open-access article distributed under the terms and conditions of the Creative Commons Attribution (CC-BY) license (http://creativecommons.org/licenses/by/4.0/).

REFERENCES

Akbari, A., Khammar, M., Taherzadeh, D., Rajabian, A., Zak, A. K. and Darroudi, M., Zinc-doped cerium oxide nanoparticles: Sol-gel synthesis, characterization, and investigation of their in vitro cytotoxicity effects, *J. Mol. Struct*., 1149, 771–776 (2017). https://doi.org/10.1016/j.molstruc.2017.08.069

Akçay, N., Algün, G. and Öztel, H. O., Fabrication of ultra-sensitive humidity sensors based on Ce-doped ZnO nanostructure with superfast response and recovery time, *J. Mater. Sci.: Mater. Electron*., 34(20), 1565 (2023). https://doi.org/10.1007/s10854-023-10973-y

Artini, C., Pani, M., Carnasciali, M. M., Buscaglia, M. T., Plaisier, J. R. and Costa, G. A., Structural Features of Sm- and Gd-Doped Ceria Studied by Synchrotron X-ray Diffraction and μ-Raman Spectroscopy, *Inorg. Chem*., 54(8), 4126–4137 (2015). https://doi.org/10.1021/acs.inorgchem.5b00395

Babu, K. S., Reddy, A. R., Sujatha, C., Reddy, K. V. and Mallika, A. N., Synthesis and optical characterization of porous ZnO, *J. Adv. Ceram*., 2(3), 260–265 (2013). https://doi.org/10.1007/s40145-013-0069-6

Bao, L. H., Lan, Y. J. and Zhang, S. F., Synthesis and Properties of Waterborne Polyurethane Dispersions with Ions in the Soft Segments, *J. Polym. Res*., 13(6), 507–514 (2006). https://doi.org/10.1007/s10965-006-9073-7

Buckman, A. B. and Kuo, C., Fizeau interferometry for measuring refractive index and thickness of nearly transparent films, *Appl. Opt*., 17(22), 3636-3640 (1978). https://doi.org/10.1364/AO.17.003636

Chai, B., Wang, X., Cheng, S., Zhou, H. and Zhang, F., One-pot triethanolamine-assisted hydrothermal synthesis of Ag/ZnO heterostructure microspheres with enhanced photocatalytic activity, *Ceram. Int*., 40(1), 429–435 (2014). https://doi.org/10.1016/j.ceramint.2013.06.019

Chen, X., Shen, Y., Zhang, W., Zhang, J., Wei, D., Lu, R., Zhu, L., Li, H. and Shen, Y., In-situ growth of ZnO nanowire arrays on the sensing electrode via a facile hydrothermal route for high-performance NO2 sensor, *Appl. Surf. Sci.,* 435, 1096–1104 (2018). https://doi.org/10.1016/j.apsusc.2017.11.222

Diao, K., Xiao, J., Zheng, Z. and Cui, X., Enhanced sensing performance and mechanism of CuO nanoparticle-loaded ZnO nanowires: Comparison with ZnO-CuO core-shell nanowires, *Appl. Surf. Sci.,* 459, 630–638 (2018). https://doi.org/10.1016/j.apsusc.2018.07.112

Elderderi, S., Loubière, C. L., Wils, L., Henry, S., Bertrand, D., Byrne, H. J., Chourpa, I., Gueiffier, C. E., Munnier, E., Elbashir, A. A., Delaye, L. B. and Bonnier, F., ATR-IR spectroscopy for rapid quantification of water content in deep eutectic solvents, *J. Mol. Liq.,* 311, 113361 (2020). https://doi.org/10.1016/j.molliq.2020.113361

Fifere, N., Airinei, A., Asandulesa, M., Rotaru, A., Ursu, E. L. and Doroftei, F., Investigating the Vibrational, Magnetic and Dielectric Properties, and Antioxidant Activity of Cerium Oxide Nanoparticles, *Int. J. Mol. Sci.,* 23(22), 13883 (2022). https://doi.org/10.3390/ijms232213883

Gao, R., Zhang, T., Zhang, X., Gao, S., Xu, Y., Cheng, X., Gao, J., Zheng, M., Zhou, X. and Huo, L., One-step controlled synthesis of ZnO-ZnSe hollow nanospheres with surface defects for selective detection of NO22, *Appl. Surf. Sci*., 635, 157628 (2023). https://doi.org/10.1016/j.apsusc.2023.157628

Ghalmi, Y., Habelhames, F., Sayah, A., Bahloul, A., Nessark, B., Shalabi, M. and Nunzi, J. M., Capacitance performance of NiO thin films synthesized by direct and pulse potentiostatic methods, *Ionics,* 25(12), 6025–6033 (2019). https://doi.org/10.1007/s11581-019-03159-2

Grinter, D. C., Allan, M., Yang, H. J., Salcedo, A., Murgida, G. E., Shaw, B. J., Pang, C. L., Idriss, H., Pirovano, V. G. and Thornton, G., Ce=O Terminated CeO_2, *Angew. Chem. Int. Ed.,* 60(25), 13835–13839 (2021). https://doi.org/10.1002/anie.202101771

He, Y., Yu, X., Li, T., Yan, L. and Yang, B., Preparation of CeO_2/ZnO nanostructured microspheres and their catalytic properties, *Powder Technol.,* 166(2), 72–76 (2006). https://doi.org/10.1016/j.powtec.2006.05.013

Heng, C. L., Wang, T., Li, H., Liu, J. J., Zhu, J. W., Ablimit, A., Su, W. Y., Wu, H. C., Yin, P. G. and Finstad, T. G., Strong enhancement of ultra-violet emission by Ce doping of ZnO sputtered films, *Mater. Lett.,* 162, 53–55 (2016). https://doi.org/10.1016/j.matlet.2015.09.125

Hussain, S., Aslam, N., Yang, X., Javed, M. S., Xu, Z., Wang, M., Liu, G. and Qiao, G., Unique polyhedron CeO_2 nanostructures for superior formaldehyde gas-sensing performances, *Ceram. Int.,* 44(16), 19624–19630 (2018). https://doi.org/10.1016/j.ceramint.2018.07.212

Jaiswal, J., Singh, P. and Chandra, R., Low-temperature highly selective and sensitive NO22 gas sensors using CdTe-functionalized ZnO filled porous Si hybrid hierarchical nanostructured thin films, *Sens. Actuators B Chem*., 327, 128862 (2021). https://doi.org/10.1016/j.snb.2020.128862

Kim, K. H., Yoshihara, Y., Abe, Y., Kawamura, M. and Kiba, T., Morphological characterization of sphere-like structured ZnO-NiO nanocomposites with annealing temperatures, *Mater. Lett.,* 186, 364–367 (2017). https://doi.org/10.1016/j.matlet.2016.10.052

Kulandaisamy, A. J., Elavalagan, V., Shankar, P., Mani, G. K., Babu, K. J. and Rayappan, J. B. B., Nanostructured Cerium-doped ZnO thin film – A breath sensor, *Ceram. Int.,* 42(16), 18289–18295 (2016). https://doi.org/10.1016/j.ceramint.2016.08.156

Li, H., Qu, Y. and Zhang, X., The gas sensor utilizing CeO_2 nanorods for the low temperature detection of hydrogen, *Inorg. Chem. Commun.,* 130, 108692 (2021). https://doi.org/10.1016/j.inoche.2021.108692

Li, R., Yabe, S., Yamashita, M., Momose, S., Yoshida, S., Yin, S. and Sato, T., Synthesis and UV-shielding properties of ZnO- and CaO-doped CeO_2 via soft solution chemical process, *Solid State Ion*., 151(1–4), 235–241 (2002). https://doi.org/10.1016/S0167-2738(02)00715-4

Lu, W., zhu, D. and xiang, X., Synthesis and properties of Ce-doped ZnO as a sensor for 1,2-propanediol, *J. Mater. Sci.: Mater. Electron.,* 28(24), 18929–18935 (2017). https://doi.org/10.1007/s10854-017-7846-x

Manisalidis, I., Stavropoulou, E., Stavropoulos, A. and Bezirtzoglou, E., Environmental and Health Impacts of Air Pollution: A Review, Front Public Health, 8, 14, (2020). https://doi.org/10.3389/fpubh.2020.00014

Mary, J. A., Vijaya, J. J., Bououdina, M. and Kennedy, L. J., Simple microwave-assisted solution combustion synthesis of cerium and nickel-doped ZnO nanostructures: Effects on structural, morphological, optical, and magnetic properties, *Superlattices Microstruct.,* 76, 174–185 (2014). https://doi.org/10.1016/j.spmi.2014.09.038

Mary, J. A., Vijaya, J. J., Bououdina, M., Kennedy, L. J., Daie, J. H. and Song, Y., Investigation of structural, surface morphological, optical properties and first-principles study on electronic and magnetic properties of (Ce, Fe)-co doped ZnO, *Phys. B Condens. Matter,* 456, 344–354 (2015). https://doi.org/10.1016/j.physb.2014.09.023

Mihály, J., Deák, R., Szigyártó, I. C., Bóta, A., Somfai, T. B. and Varga, Z., Characterization of extracellular vesicles by IR spectroscopy: Fast and simple classification based on amide and C-H stretching vibrations, *Biochim. et Biophys. Acta (BBA)-Biomembr.,* 1859(3), 459–466 (2017). https://doi.org/10.1016/j.bbamem.2016.12.005

Moslehnejad, N., Jahangiri, M., Vafaee, F. and Niasari, M. S., Synthesis and characterization of ZnO–Ce nanophotocatalyst and their application for the removal of dye (Reactive red 198) by degradation process: Kinetics, thermodynamics and experimental design, *Int. J. Hydrogen Energy*, 47(57), 23980–23993 (2022). https://doi.org/10.1016/j.ijhydene.2022.05.189

Nandiyanto, A. B. D., Oktiani, R. and Ragadhita, R., How to read and interpret FTIR spectroscope of organic material, Indones, *J. Sci. Technol*., 4(1), 97–118 (2019). https://doi.org/10.17509/ijost.v4i1.15806

Naqvi, A. M. S., Soleimani, H., Yahya, N. and Irshad, K., Structural and optical properties of chromium-doped zinc oxide nanoparticles synthesized by sol-gel method, *AIP Conf. Proc.,* 1621, 530–537 (2014). https://doi.org/10.1063/1.4898517

Orellano, P., Reynoso, J., Quaranta, N., Bardach, A. and Ciapponi, A., Short-term exposure to particulate matter (PM_{10} and $PM_{2.5}$), nitrogen dioxide (NO_2), and ozone (O_3) and all-cause and cause-specific mortality: Systematic review and meta-analysis, *Environ. Int.,* 142, 105876 (2020). https://doi.org/10.1016/j.envint.2020.105876

Debye P. and Scherrer, P., Interference of irregularly oriented particles in X-rays, *Phys. Ziet*,17, 277–283, (1916)

Petruci, J. F. S., Tütüncü, E., Cardoso, A. A. and Mizaikoff, B., Real-time and simultaneous monitoring of NO, NO2, and N2O using substrate–integrated hollow waveguides coupled to a compact Fourier transform infrared (FT-IR) spectrometer, *Appl. Spectrosc*., 73(1), 98–103 (2019). https://doi.org/10.1364/AS.73.000098

Prakoso, S. P., Paramarta, V., Tju, H., Taufik, A. and Saleh, R., The influence of narrow optical gap silver oxide on zinc oxide nanoparticles produced by microwave-assisted colloidal synthesis: photocatalytic studies, *J. Phys. Conf. Ser*., 776, 012051 (2016). https://doi.org/10.1088/1742-6596/776/1/012051

Reddy, P. R., Jayarambabu, N., Somasai, A. K., Rao, K. V., and Aparna, Y., Structural and Morphological Studies of ZnO-CeO_2 Nanocomposites, *Mater. Today Proc*., 3(10), 4146–4150 (2016). https://doi.org/10.1016/j.matpr.2016.11.088

Saranya, S., Sethupathi, N., Mahalingam, P. and Sivakumar, P., Characterization and Ambiennt temperature Hydrogen Sulfide Sensing of Annealed NiO- MnO2 Thin Films Prepared via Jet Nebulizer Spray Pyrolysis, *J. Environ. Nanotechnol*., 13(3), 133-139(2024). https://doi.org/10.13074/jent.2024.09.242717

Sharma, D. K., Sharma, K. K., Kumar, V. and Sharma, A., Effect of Ce doping on the structural, optical and magnetic properties of ZnO nanoparticles, *J. Mater. Sci.: Mater. Electron.,* 27(10), 10330–10335 (2016). https://doi.org/10.1007/s10854-016-5117-x

Shukla, S. K., Agorku, E. S., Mittal, H. and Mishra, A. K., Synthesis, characterization and photoluminescence properties of Ce^{3+}-doped ZnO-nanophosphors, *Chem. Pap.,* 68(2), 217-222 (2013). https://doi.org/10.2478/s11696-013-0442-5

Shulga, A., Butusov, L., Chudinova, G. K. and Sheshko, T., Microwave-Assisted Synthesis of Cerium Doped ZnO Nanostructures and Its Optical Properties, *J. Phys. Conf. Ser.,* 1461(1), 012162 (2020). https://doi.org/10.1088/1742-6596/1461/1/012162

Sofiani, Z., Derkowska, B., Dalasiński, P., Wojdyła, M., Seignon, D. S., Lamrani, M. A., Dghoughi, L., Bała, W., Addou, M. and Sahraoui, B., Optical properties of ZnO and ZnO:Ce layers grown by spray pyrolysis, *Opt. Commun*., 267(2), 433–439 (2006). https://doi.org/10.1016/j.optcom.2006.06.049

Srinivasan, M. P., Uthiram, C., Ayeshamariam, A., Kaviyarasu, K. and Punithavelan, N., Dielectric performance of CeO_2/ZnO core–shell nanocomposite with their structural, optical and morphological properties, *J. King Saud Univ. Sci*., 35(2), 102508 (2023). https://doi.org/10.1016/j.jksus.2022.102508

Sui, L., Yu, T., Zhao, D., Cheng, X., Zhang, X., Wang, P., Xu, Y., Gao, S., Zhao, H., Gao, Y. and Huo, L., In situ deposited hierarchical CuO/NiO nanowall arrays film sensor with enhanced gas sensing performance to 2, *J. Hazard. Mater.,* 385, 121570 (2020). https://doi.org/10.1016/j.jhazmat.2019.121570

Sun, K., Zhan, G., Zhang, L., Wang, Z. and Lin, S., Highly sensitive NO2 gas sensor based on ZnO nanoarray modulated by oxygen vacancy with Ce doping, *Sens. Actuators B Chem*., 379, 133294 (2023). https://doi.org/10.1016/j.snb.2023.133294

Tauc, J., Grigorovici, R. and Vancu, A., Optical Properties and Electronic Structure of Amorphous Germanium, *Phys. Status Solidi B*, 15(2), 627–637 (1966). https://doi.org/10.1002/pssb.19660150224

Tsai, Y. T., Chang, S. J., Ji, L. W., Hsiao, Y. J., Tang, I. T., Lu, H. Y. and Chu, Y. L., High Sensitivity of NO Gas Sensors Based on Novel Ag-Doped ZnO Nanoflowers Enhanced with a UV Light-Emitting Diode, *ACS Omega*, 3(10), 13798–13807 (2018). https://doi.org/10.1021/acsomega.8b01882

Verma, K. C. and Kotnala, R. K., Defects-assisted ferromagnetism due to bound magnetic polarons in Ce into Fe, Co:ZnO nanoparticles and first-principle calculations, *Phys. Chem. Chem. Phys*., 18(7), 5647–5657 (2016). https://doi.org/10.1039/C5CP06930K

Xin, M., Crystal Structure and Optical Properties of ZnO:Ce Nano Film, *Mol*., 27(16), 5308 (2022). https://doi.org/10.3390/molecules27165308

Xu, Y. N. and Ching, W. Y., Electronic, optical, and structural properties of some wurtzite crystals, *Phys. Rev. B,* 48(7), 4335–4351 (1993). https://doi.org/10.1103/PhysRevB.48.4335

Zhang, J., Chen, T., Yu, J., Liu, C., Yang, Z., Lu, H., Yin, F., Gao, J., Liu, Q., Zhang, X. and Tu, Y., Enhanced photocatalytic activity of flowerlike CuO–ZnO nanocomposites synthesized by one-step hydrothermal method, *J. Mater. Sci.: Mater. Electron*., 27(10), 10667–10672 (2016). https://doi.org/10.1007/s10854-016-5166-1

Zhang, Y. G., Zhang, G. B. and Wang, Y. X., First-principles study of the electronic structure and optical properties of Ce-doped ZnO, *J. Appl. Phys.,* 109(6), 063510 (2011). https://doi.org/10.1063/1.3561436